

## Halo evolution in a cosmological environment

S. Gottlöber<sup>1</sup>

*Astrophysical Institute Potsdam, An der Sternwarte 16, D-14482  
Potsdam, Germany*

A.A. Klypin, A.V. Kravtsov

*Astronomy Department, NMSU, Dept.4500, Las Cruces, NM  
88003-0001, USA*

### Abstract.

We present results of a study of the formation and evolution of the dark matter (DM) halos in a *COBE*-normalized spatially flat  $\Lambda$ CDM model ( $\Omega_0 = 1 - \Omega_\Lambda = 0.3$ ;  $h = 0.7$ ). The dynamics of  $256^3$  DM particles is followed numerically in a box of  $60h^{-1}$  Mpc with the dynamic range of 32,000 in spatial resolution. The high resolution of the simulation allows us to examine evolution of both *isolated* and *satellite* halos in a representative volume. We discuss the new halo finding algorithm designed to identify halos in high-density environments, present results on the evolution of velocity function of DM halos and compare it with the Press-Schechter function, discuss the evolution of power spectrum of matter and halo distributions, and mass evolution of halos.

The velocity function of halos at  $z = 0$  compares well with the prediction of the Press-Schechter approximation, but for circular velocities in the range 100 – 200 km/s simulations predict  $\sim 1.3$  time more halos (mostly in clusters or groups). In real space the power spectra of halos and DM are very different (halos are anti-biased). Both spectra do not have simple power-law shape. In redshift space the spectra are close to a power law with  $\gamma = -2.1$  in the range of wave numbers  $k = 0.2 - 5h\text{Mpc}^{-1}$ . The power spectra of halo distribution evolves only mildly for  $z = 0 - 3$ . The mass evolution of *isolated* virialized objects determined from the simulation is in good agreement with predictions of the extended Press-Schechter models. However, satellite halos evolve very different: for some of them the mass decreases with time, which happens if the halos fall into clusters or groups. We discuss the dependence of the correlation function of halo populations on their environment and merging history.

---

<sup>1</sup>Also: Astronomy Department, NMSU, Dept.4500, Las Cruces, NM 88003-0001

## 1. Introduction

A variety of observations on a wide range of spatial scales (i.e. rotation curves of galaxies, galaxy dynamics and gravitational lensing in galaxy clusters, the large-scale velocity flows, etc.) indicate the existence of dark matter (DM) in the Universe. The total amount of DM is not yet known, but it is generally believed that cold dark matter dominates the mass in the Universe and significantly affects both the process of galaxy formation and the large-scale distribution of galaxies. The gravitational domination of DM on the scale of galactic virial radius implies that collisionless simulations can be used to study formation of the DM component of galaxies.

It is well known that cosmological scenarios with cold dark matter alone cannot explain the structure formation both on small and very large scales. Recently, scenarios with a non-zero vacuum energy, quantified by the cosmological constant  $\Lambda$ , have been proved to be very successful in describing most of the observational data at both low and high redshifts. In this contribution, we discuss the evolution of DM halos in a spatially flat cosmological model dominated by the cosmological constant and cold dark matter,  $\Lambda$ CDM. A simulated box of  $60 h^{-1}$  Mpc size allows to construct and study statistically representative halo catalogs (about 10,000 halos are identified at  $z = 0$ ). The novel feature of this analysis is study of both isolated and satellite halos, where halos are dubbed satellites if they are located within the virial radius of a larger host system (massive galaxies or galaxy groups and clusters). This allows us to study the differences between isolated and satellite halos; here we discuss the differences in their mass evolution and spatial distribution.

## 2. Numerical simulation

We simulate the evolution of  $256^3$  cold dark matter particles in a spatially flat model with a cosmological constant ( $\Lambda$ CDM;  $\Omega_0 = 1 - \Omega_\Lambda = 0.3$ ;  $\sigma_8 = 1.0$ ;  $H_0 = 70$  km/s/Mpc). The model is normalized in accord with the four year COBE DMR observations (Bunn & White 1997) and observed abundance of galaxy clusters (Viana & Liddle 1996). The age of the universe in this model is  $\approx 13.5$  Gyrs.

In order to study the statistical properties of halos in a cosmological environment, the simulation box should be sufficiently large. On the other hand, to assure that halo survival in clusters, the force resolution should be  $\lesssim 1 - 3h^{-1}$  kpc and the mass resolution should be  $\lesssim 10^9 h^{-1} M_\odot$  (Moore et al. 1996, Klypin et al. 1998, hereafter KGKK). The simulations were done using the Adaptive Refinement Tree (ART) code (Kravtsov, Klypin & Khokhlov 1997). The code used a  $512^3$  homogeneous grid on the lowest level of resolution and six levels of refinement, each successive refinement level doubling the resolution. The sixth refinement level corresponds to a formal dynamical range of 32,000 in high density regions. Thus we can reach in a  $60 h^{-1}$  Mpc box the force resolution of  $\approx 2h^{-1}$  kpc. The simulation has a mass resolution (particle mass of  $1.1 \times 10^9 h^{-1} M_\odot$ ) sufficient to identify galaxy-size halos ( $M \gtrsim 3 \times 10^{10} h^{-1} M_\odot$ ).

The ART code integrates the equations of motion in *comoving* coordinates. However, its refinement strategy is designed to effectively preserve the initial

*physical* resolution of the simulation. In order to prevent degradation of force resolution in *physical* coordinates, the dynamic range between the start ( $z_i = 30$ ) and the end of the simulation should increase by  $(1 + z_i)$ : For our simulations it should have at least the dynamical range  $512 \times (1 + z_i) = 15,872$ . This is accomplished with the prompt successive refinements *in high-density regions* during the simulations. The peak resolution is reached by creating a hierarchy with six levels of refinement. The spatial refinement is accompanied by the similar refinement of the integration time step. The integration step of  $\Delta a_0 = 0.0015$  corresponds to 645 time steps on the lowest-resolution of the uniform grid and to (effective) 41,280 on the deepest refinement level. In physical units, the latter step corresponds to  $2.3 \times 10^9$  years.

### 3. Challenges in halo identification

Identification of halos in dense environments and reconstruction of their evolution is a challenge. Any halo finding algorithm has to deal with difficult “decision-making” situations, existing also in the real Universe. The most typical difficulties arise if a small satellite is bound to a larger galaxy (like the LMC and the Milky Way or the M51 system) or in cases when many small gravitationally self-bound halos are moving within a large region of virial overdensity (galaxy clusters and groups).

Assuming that the satellite is self-gravitationally bound, we would have to include the mass of the satellite in the mass of the host system. By doing so, we count mass of the satellite twice: when we identify the satellite and when we identify the host system. This may seem unreasonable, but if we do not include the satellite, then the mass of the large galaxy is underestimated. For example, the binding energy of a particle at the distance of the satellite will be wrong. The problems arise also when we try to assign particles to different halos in the effort to find halo masses. This is very difficult to do for particles moving between halos. Even if a particle at some moment is bound to one of the halos, it is not guaranteed that it belongs to the halo. The gravitational potential changes with time, and the particle may end up falling onto another halo. These effects are especially frequent in high-density crowded regions typical of galaxy groups and clusters. This situation actually was observed very often in simulated halos when we compared particle contents of halos at different redshifts. It represents an additional difficulty in tracing the mass history of such halos.

It is also difficult to estimate the actual mass of a halo orbiting inside a cluster-size object. The formal virial radius of such a satellite halo is simply equal to the cluster’s virial radius. We have chosen to define the outer *tidal* radius of the satellite halos as a scale at which their density profile starts to flatten. At small distances from the center of the satellite the density steeply declines, but then it flattens out and may even increase. This means that we reached the outer border of the satellite. The corresponding mass within tidal radius is then our approximation to the halo mass. With these considerations in mind, the halo finding algorithm must allow halos to overlap and DM particles to belong to more than one halo.

#### 4. Halo finding algorithm

The most widely used halo-finding algorithms, the friends-of-friends (FOF) and the spherical overdensity, both discard “halos inside halos”, i.e., satellite halos located within the virial radius of larger halos. The distribution of halos identified in this way, cannot be compared easily to the distribution of galaxies, because the latter are found within larger systems. In order to cure this, we have developed two related algorithms, which we called the *hierarchical friends-of-friends* (HFOF) and the *bound density maxima* (BDM) algorithms (KGKK).

Since the algorithms work on a snapshot of the particle distribution, they tend to identify also small fake “halos” consisting of only a few *unbound* particles, clumped together by chance at the analyzed moment. We deal with this problem by both checking whether the identified clump is gravitationally bound and by following the merging history of halos. A halo that does not have a progenitor at the previous moment is discarded, if the particles from which this halo has been formed belong at the previous moment already to other halos. In this case the halo is assumed to be a fake one. If it has formed from single particles or small objects below the threshold of halo detection, it is assumed that a new halo has been formed. For other halos we find the direct progenitor, i.e. a halo at a previous moment that contains the maximum number of particles of this halo. We use the chain of progenitors identified in this way to reconstruct the mass evolution of the given halo back in time, down to the epoch of its first detection in the simulation.

The HFOF and BDM algorithms are complementary. Both of them find essentially the same halos. Therefore, we believe that each of them is a stable algorithm which finds in a given dark matter distribution all dark matter halos above a given mass threshold. The advantage of the HFOF algorithm is that it can handle halos of arbitrary, not only spherically symmetric, shape. The advantage of the BDM algorithm is that it describes better the physical properties of the halos due to the fact that it separates background unbound particles from the particles gravitationally bound to the halo.

#### 5. Velocity function

Interacting halos exchange mass and lose mass. The total mass of a halo depends on its radius which, as was pointed out above, is difficult to define. We try to avoid this problem by assigning not only a mass to a halo, but finding also its maximum “circular velocity” ( $\sqrt{GM/R}$ ),  $v_{circ}$ . This is the quantity which is more meaningful observationally. Numerically,  $v_{circ}$  can be measured more easily and more accurately than mass.

The output of the halo finding algorithm depends primarily on the assumed mass threshold. With the threshold of  $10^{10}h^{-1}M_{\odot}$  (10 particles) the algorithm identifies  $\sim 17000$  halos, whereas a mass threshold of  $3 \times 10^{10}h^{-1}M_{\odot}$  (28 particles) results in identification of more than 9000 halos. There is a weak dependence on the assumed maximum halo radius (2% decrease if changing the maximum radius from  $100h^{-1}$  kpc to  $150h^{-1}$  kpc).

For any study one needs to have a complete halo sample that is not affected by the numerical details of halo finding procedure. In order to test the complete-

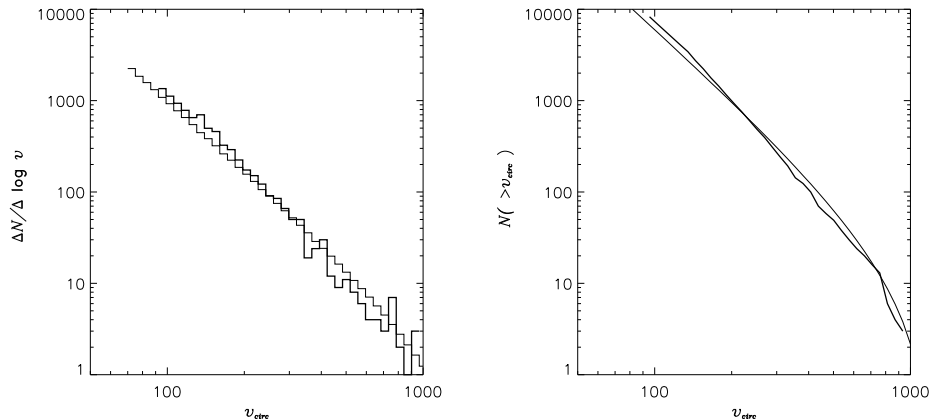


Figure 1. Differential (left panel) and integral (right panel) velocity functions of halos at  $z = 0$ . The thick lines show the velocity function of halos, while thin lines represent the Press-Schechter prediction.

ness of the halo samples, we have constructed the differential velocity functions at  $z = 0$  for different mass thresholds and maximum radii. We find that the halo samples do not depend on the numerical parameters of the halo finder for halos with  $v_{circ} \gtrsim 100$  km/s. Particularly, the differential velocity function for  $v_{circ} > 100$  km/s is robust and does not depend on the assumptions. There is a substantial scatter for  $v_{circ} > 500$  km/s where we have less than 10 halos per logarithmic velocity bin. In fact, increasing the maximum halo radius one (slightly) increases also the maximum circular velocity, if it is not yet reached. This is the case for the most massive halos. We reanalyzed these halos and found that in all cases the maximum circular velocity changed by less than 10 %.

In Figure 1, we compare the velocity function of halos in our simulation with the Press-Schechter (PS) prediction. The latter has been computed by converting virial mass in the PS mass function to  $v_{circ}$ , assuming the NFW density profile of the halos. There is an excess of small halos ( $v_{circ} < 200$  km/s) over the PS prediction. This is expected because we include satellite halos in our catalog, while PS model predicts mass function of the isolated objects. For higher circular velocities we find a slight deficit of massive halos (20% - 30 %) in comparison with the numbers predicted by the PS mass function. In particular, for the largest halos, the over-prediction may be influenced by the assumption of NFW density profile which is a rather poor description for some of the large halos with substantial central sub-structure. The prediction of the simulation is also influenced by cosmic variance in our single realization; we may have a deficit of massive halos in the given realization just by chance.

## 6. Halo evolution

In the following we will discuss first the evolution of halo clustering and then the evolution of the halos. We consider three catalogs of halos with  $v_{circ} > 120$  km/s at  $z = 0, 1, 3$  (4804, 8018, 8396 halos respectively). These samples are

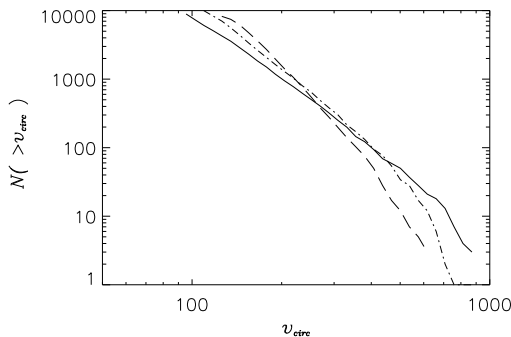


Figure 2. Evolution of the integral velocity function of halos. The solid, dot-dashed, and dashed curves correspond to  $z = 0$ ,  $z = 1$ , and  $z = 3$ , respectively.

are complete for  $z = 0, 1$ : the differential velocity function does not show any turnoff (see Figure 2) at these velocities. We are missing part of the halos with  $v_{circ} < 130$  km/s at  $z = 3$ . To study the evolution of the halos we construct the mass evolution history of all halos which have been identified in the simulation at  $z = 0$ .

### 6.1. Evolution of halo clustering

In Figures 3 and 4, we show the evolution of the power spectrum of these halos in comparison with the power spectrum of the DM particles. We have calculated the power spectrum on a  $512^3$  grid; the spectra are shown up to half of the Nyquist frequency  $k_{box} \times 128$ . The shot noise level  $S = V/N$  for the halo samples is 45, 27, and 26, respectively. The shot noise power derived from a random distribution is constant up to about a quarter of the Nyquist frequency  $k_{box} \times 64$  and decrease than by about 25%. We expect an error of the same order in the halo power spectrum at  $k_{box} \times 128$ .

The halo power spectrum evolves much slower than that of the dark matter. The halos are clearly biased at  $z = 3$ , are essentially unbiased at  $z = 1$ , and are anti-biased at  $z = 0$ . A detailed analysis of the evolution of halo and matter power spectra and bias will be presented elsewhere (Kravtsov and Klypin 1998, in preparation). The results obtained from the power spectrum analysis are in qualitative agreement with results on the bias evolution as derived from the correlation function analysis by Colín et al. (1998) and other researchers. The scale dependence of the bias, however, is quite different.

In the right panels of Figures 3 and 4, we show the power spectrum of halos and dark matter in *redshift* space. The redshift space power spectra are always much steeper than in real space. At  $z = 0$ , the real space power spectrum of dark matter shows a clear excess over the linear power spectrum due to nonlinear clustering. The corresponding dark matter power spectrum in redshift space follows almost exactly the linear power spectrum of dark matter.

In real space the power spectra of halos and DM are very different. Both spectra do not have a simple power-law shape. The real-space power spectrum

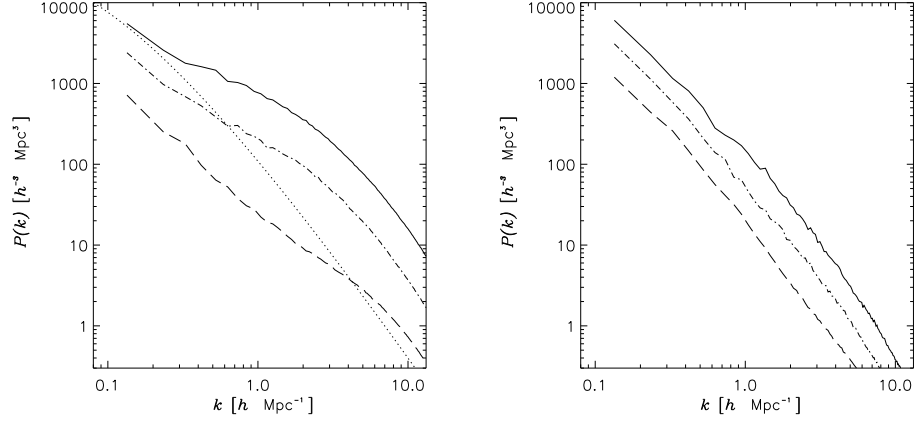


Figure 3. Evolution of real-space (left) and redshift-space (right) power spectrum of the DM particles. The solid, dot-dashed, and dashed curves correspond to  $z = 0$ ,  $z = 1$ , and  $z = 3$ , respectively. The dotted line left shows the linear power spectrum at  $z = 0$ .

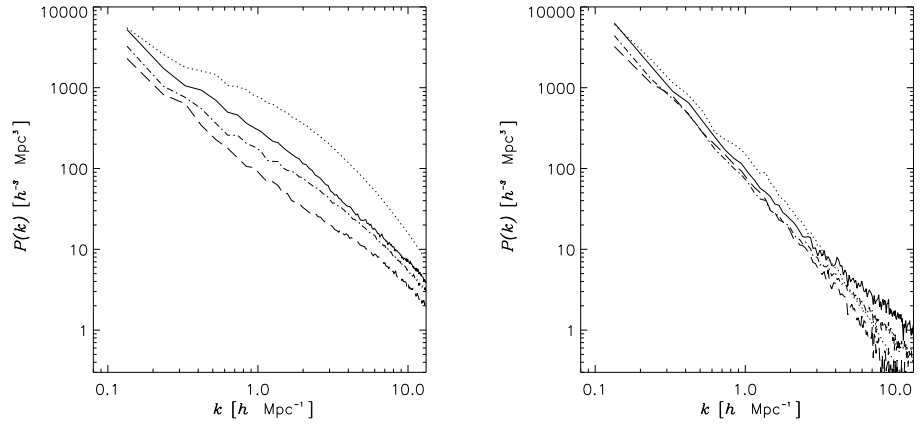


Figure 4. Evolution of real-space (left) and redshift-space (right) power spectrum of halos with circular velocity  $v_{circ} > 120$  km/s. The solid, dot-dashed, and dashed curves correspond to  $z = 0$ ,  $z = 1$ , and  $z = 3$ , respectively. The dotted lines show the DM power spectrum at  $z = 0$ .

of halo distribution evolves only mildly between  $z = 3$  and  $z = 0$ . Similarly to the real space case, the redshift-space power spectrum of halos shows almost no evolution during this time. In the range of wave numbers  $k = 0.2 - 5h \text{ Mpc}^{-1}$  the redshift space power spectrum of halos is close to a power law with  $\gamma = -2.1$ . A power spectrum slope of  $\sim -2.1$  had been measured for the combined SSRS2 + CfA2 galaxy sample on scales  $\lesssim 30h^{-1} \text{ Mpc}$  (da Costa et al. 1994).

## 6.2. Progenitors of halos

In order to study the evolution of individual halos, we need to construct a complete evolution tree for each of the halos in the  $z = 0$  catalog. We proceed as follows: We have selected 19 epochs ( $z = 0, 0.05, 0.1, 0.2, 0.3, 0.4, 0.5, 0.6, 0.7, 0.8, 0.9, 1.0, 1.5, 2., 2.5, 3., 5., 10., 15.$ ). For every epoch, we identify a progenitor of a  $z = 0$  halo. The procedure of progenitor identification is based on the comparison of lists of particles belonging to the halos at different moments both back and forward in time. As was mentioned above, the halo finder algorithm allows halos to overlap, or, in other words allows particles to belong to more than one halo. The visual inspection of a large number of constructed evolution trees showed that this forward-backward algorithm of tracing halo histories identifies the correct “ancestor-descendant” relationships rather accurately, with obvious ancestor-descendant misidentifications in  $\lesssim 2\%$  of the cases.

Using the procedure described above, we are able to address the question of the *halo detection epoch*, which we define as an epoch at which the halo has been identified for the first time. The epoch of the first identification depends, of course, on the mass threshold assumed by the halo finder. The following results are for the lowest possible mass  $3 \times 10^{10} h^{-1} M_{\odot}$  at  $z = 0$ . For this mass threshold the halo catalog is dominated by halos of mass  $\lesssim 10^{11} h^{-1} M_{\odot}$ , which fall below the identification threshold quickly as we trace their mass evolution back in time. The distribution of detection time for these halos is thus likely to reflect selection function determined by the threshold rather than any kind of physical “formation epoch” distribution. In the left panel of Figure 5, we show the distribution of detection epochs for the halos identified with mass threshold of  $3 \times 10^{10} h^{-1} M_{\odot}$ . The number of progenitors at a given redshift exponentially decreases with redshift. The figure shows that the first halo in this catalog should have been detected as early as  $z = 10$ . Indeed, at  $z = 10$  we find one halo of mass  $1.95 \times 10^{11} M_{\odot}$  (184 bound particles shown as filled circles in the right panel of Figure 5). The overdensity of the halo is 400 which means that it is a virialized object. We show also the surrounding, not yet bound, particles of the halo (open circles). The overdensity in the box of  $400h^{-1} \text{ kpc}$  size centered on this object is  $\approx 50$ . The figure also shows a flattened structure of the particle distribution: the halo forms inside of a small pancake.

## 6.3. Halo mass evolution and environment

The mass of an object found by the HFOF algorithm *at virial overdensity* can be defined as the sum of linked particle masses. In this case we do not only find galaxy size halos but also all group size and cluster size halos. For all of the HFOF objects we identify the main progenitors at all epochs down to the halo detection time. To study the mass evolution due to merging and accretion we have divided these objects into three mass bins at  $z = 0$ . The average

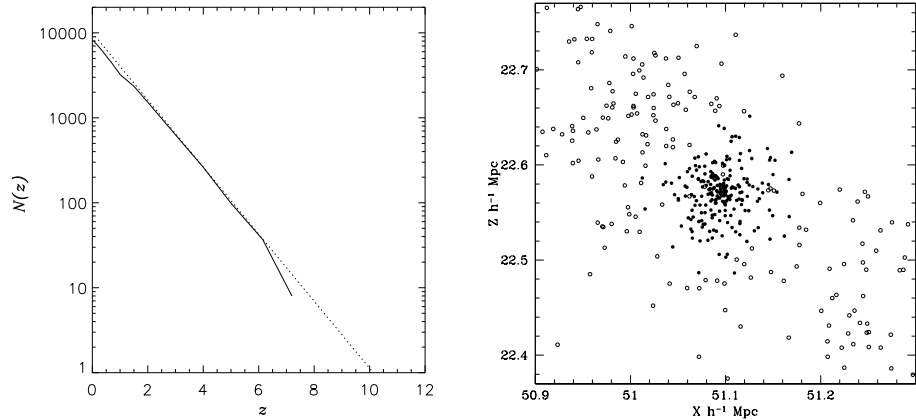


Figure 5. Left: Number of halos in a  $60h^{-1}\text{Mpc}$  simulation box whose progenitors existed at redshift  $z$ . Only halos with mass larger than  $3 \times 10^{10}h^{-1}\text{M}_{\odot}$  have been taken into account. Dotted line:  $\propto \exp(-z/z_1)$ ,  $z_1 = 1.1$ . Right: A virialized halo ( $M \approx 1.95 \times 10^{11}\text{M}_{\odot}$ ) at  $z = 10$ ; filled circles show particles bound to the halo, the open circles show unbound particles.

mass evolution of halos in these bins normalized to the mass at  $z = 0$  is shown in Figure 6, left. The dotted line is for average halo mass of  $1.2 \times 10^{13}\text{M}_{\odot}$  (12 halos), the dashed for  $1.0 \times 10^{12}\text{M}_{\odot}$  (17 halos), the dash-dotted for  $1.1 \times 10^{11}\text{M}_{\odot}$  (265 halos). The solid lines show the predictions of semi-analytical model (kindly provided by Claudio Firmani) for  $10^{13}$ ,  $10^{12}$ , and  $10^{11}\text{M}_{\odot}$ , from the bottom to the top. We find a good agreement with the semi-analytical predictions (Lacey & Cole 1993) for the evolution of the FOF selected objects, which are per definition isolated.

Unfortunately, there is no simple and straightforward way to assign a mass for all halos identified in the simulation. Unlike the isolated halos identified by HFOF at virial overdensity, the satellite halos, although surviving, are subject to tidal stripping which reduces their mass. They are limited therefore by tidal, rather than virial, radius. To assign masses to the halos we proceed as follows. The isolated halos are assigned the mass inside the virial radius or radius of  $100h^{-1}$  kpc, whichever is smaller. The satellite halos are assigned the total mass of *gravitationally bound* particles within their tidal radius (or, again, within  $100h^{-1}$  kpc, whichever is smaller). The tidal radius is determined as the radius at which the density profile of a halo flattens (stops decreasing).

We now construct the complete mass evolution histories for the set of *all* halos with the masses assigned as described above. We have divided these halos into five groups with masses  $M_0 > 10^{13}\text{M}_{\odot}$ ,  $10^{13}\text{M}_{\odot} > M_0 > 5 \times 10^{12}\text{M}_{\odot}$ ,  $5 \times 10^{12}\text{M}_{\odot} > M_0 > 10^{12}\text{M}_{\odot}$ ,  $10^{12}\text{M}_{\odot} > M_0 > 5 \times 10^{11}\text{M}_{\odot}$ , and  $5 \times 10^{11}\text{M}_{\odot} > M_0$ . We defined a subset of 3674 halos, mass of which increases (with allowance for small statistical fluctuations) at all epochs. As before, the mass of these objects is normalized to their final mass at  $z = 0$ . The mass evolution of these halos is shown in Figure 6, right (solid lines). The solid lines are for average masses of

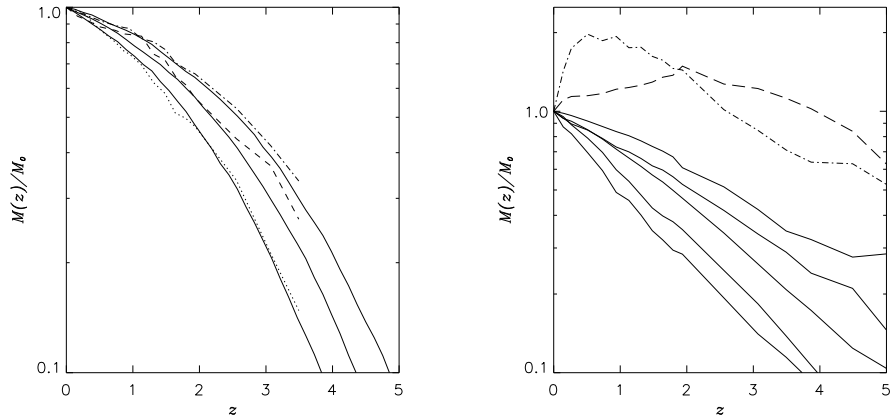


Figure 6. Left: Mass evolution of isolated objects identified by the HFOF algorithm at virial overdensity. The thin lines are for different average masses of these objects (see text). The solid lines show the predictions of the extended Press-Schechter approximation for different masses (see text). Right: Mass evolution of all halos. The solid lines are for different average masses (see text), the dot-dashed and the dashed lines show the mass evolution of a subset of halos which loose mass due to the tidal interaction. The radius of the halos was restricted to be not more than  $100 h^{-1}$  kpc.

(from the bottom to the top)  $1.2 \times 10^{13} M_{\odot}$  (14 halos),  $6.6 \times 10^{12} M_{\odot}$  (34 halos),  $1.9 \times 10^{12} M_{\odot}$  (442 halos),  $7.0 \times 10^{11} M_{\odot}$  (534 halos), and  $2.4 \times 10^{11} M_{\odot}$  (2650 halos). The overall evolution is similar to the mass evolution of isolated halos described above Figure 6, left). Note, however, that while the mass evolution tracks are curved in Figure 6, left, the mass evolution of the sample that includes satellites can be better represented by the straight lines in these log-log plots. This difference is due to the different halo selection procedure and to the different assignment of mass to the selected halos.

In the two lowest mass ranges we also find an additional subset of 2650 halos, whose masses decrease after  $z = 1$ : The dot-dashed (average mass of  $6.9 \times 10^{11} M_{\odot}$ ) and the dashed (average mass of  $2.0 \times 10^{11} M_{\odot}$ ) lines in Figure 6 (right) show the mass evolution of this subset of halos which loose mass due to the tidal stripping in groups and clusters.

Their mass increases at high redshifts, reaches a maximum and decreases thereafter. Contrary to the main halo population, the mass of which always increases (*merging halos*) the mass of these *stripped* halos grows first due to accretion of surrounding material and of smaller halos. At some point, however, these halos start to loose mass due to either tidal stripping or interaction with other nearby halos. In the left panel of Figure 7, we show the distribution of these halo subsets at  $z = 1$  and  $z = 0$ . At  $z = 1$  the “stripped” halos are distributed similarly to the rest of the halos. At  $z = 0$ , however, they are clustered much more strongly than the overall halo population.

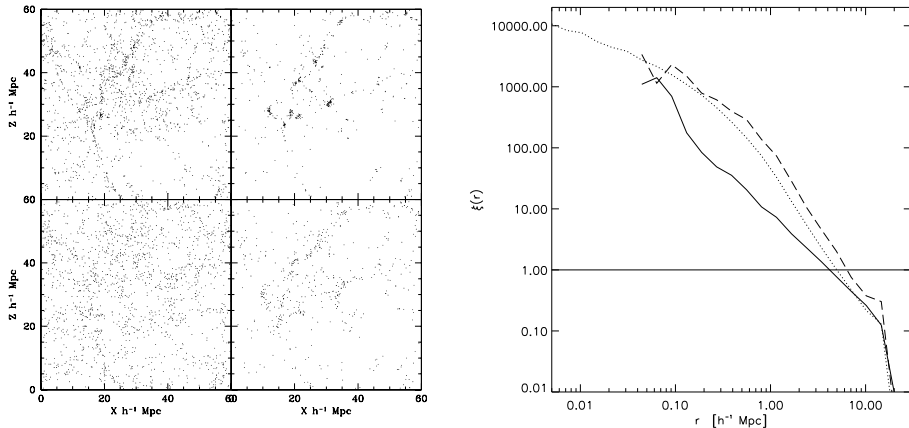


Figure 7. Left: A slice of  $15h^{-1}$  Mpc thickness: Merging (left) and stripped (right) halos at  $z = 0$  (top row), the same halos at  $z = 1$  (bottom row). Right: The correlation function of halos with circular velocities  $v_{circ} > 120$  km/s at  $z = 0$ . The solid line corresponds to halos the mass of which always increases (solid lines in Figure 6, right), the dashed line corresponds to halos which loose mass during evolution (dashed and dashed-dotted lines in Figure 6, right). The correlation function of dark matter particles is shown by the dotted line.

In the right panel of Figure 7, we show the correlation function for the two subsets of halos: always increasing mass and decreasing mass at  $z < 1$ . The correlation functions of the former has a lower amplitude and is not as steep as the correlation function of the latter. Note that the CF of the halos with the ever-increasing mass is anti-biased at scales  $\lesssim 10h^{-1}$  Mpc, the CF of the halos that loose mass is actually positively biased. This reflects the fact that the loosing mass halos are found within massive systems such as massive galaxies, groups, and clusters, and are therefore strongly clustered.

One might speculate that this difference in the correlation functions may serve as a possible explanation for the color segregation of the correlation amplitude that has been recently observed (Carlberg et al. 1998). In fact, one could expect that the galaxies hosting halos which undergo different mass evolution also show different properties, and colors in particular. Further studies are necessary to test whether this simple picture can really explain the observations.

**Acknowledgments.** This work was funded by the NSF and NASA grants to NMSU. SG acknowledges support from Deutsche Akademie der Naturforscher Leopoldina with means of the Bundesministerium für Bildung und Forschung grant LPD 1996. We acknowledge support by NATO grant CRG 972148. We thank Claudio Firmani and Vladimir Avila-Reese for providing mass evolution predictions of semi-analytical models. The numerical simulations has been carried out at the Origin2000 computers at NCSA and Naval Research Laboratory (NRL).

## References

- Bunn E.F., White M., 1997, ApJ 480, 6
- Carlberg R.G. et al., 1997, Phil. Trans. R. Soc. Lond. A, submitted, astro-ph/9805131
- Colín P., Klypin A.A., Kravtsov A.V., Khokhlov A.M., 1998, ApJ, submitted, astro-ph/9809202
- da Costa L.N., Vogeley M.S., Geller J.G., Huchra J.P., Park C., 1994, ApJ, 437, L1
- Klypin A.A., Gottlöber S., Kravtsov A.V., Khokhlov A.M., 1998, ApJ, submitted, astro-ph/9708191 (KGKK)
- Lacey C., Cole S. 1993, MNRAS, 262, 627
- Moore B., Katz N., Lake G., 1996, ApJ, 457, 455
- Viana P.T.P., Liddle A. 1996, MNRAS, 281, 323